Article

Temperature Triggered Self-Assembly of Polypeptides into Multivalent Spherical Micelles

Matthew R. Dreher, Andrew J. Simnick, Karl Fischer, Richard J. Smith, Anand Patel, Manfred Schmidt, and Ashutosh Chilkoti

J. Am. Chem. Soc., **2008**, 130 (2), 687-694 • DOI: 10.1021/ja0764862

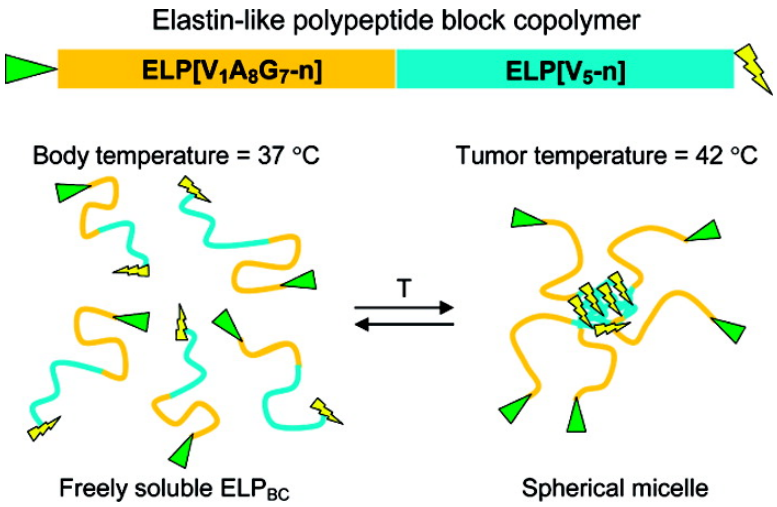

More About This Article

Additional resources and features associated with this article are available within the HTML version:

- Supporting Information
- Links to the 2 articles that cite this article, as of the time of this article download
- Access to high resolution figures
- Links to articles and content related to this article
- Copyright permission to reproduce figures and/or text from this article

View the Full Text HTML

J|A|C|S
ARTICLES
Published on Web 12/18/2007

Temperature Triggered Self-Assembly of Polypeptides into Multivalent Spherical Micelles

Matthew R. Dreher,[†,‡] Andrew J. Simnick,[†] Karl Fischer,[§] Richard J. Smith,[†] Anand Patel,[†] Manfred Schmidt,[§] and Ashutosh Chilkoti*[,†]

Department of Biomedical Engineering, Duke University, Durham, North Carolina 27708, National Institutes of Health, Clinical Center, Diagnostic Radiology Department, Bethesda, Maryland 20892, and Institut für Physikalische Chemie, Johannes Gutenberg-Universität, Mainz, Germany

Received August 28, 2007; Revised Manuscript Received November 7, 2007; E-mail: chilkoti@duke.edu

Abstract: We report herein thermally responsive elastin-like polypeptides (ELPs) in a linear AB diblock architecture with an N-terminal peptide ligand that self-assemble into spherical micelles when heated slightly above body temperature. A series of 10 ELP block copolymers (ELP_{BC}'s) with different molecular weights and hydrophilic-to-hydrophobic block ratios were genetically synthesized by recursive directional ligation. The self-assembly of these polymers from unimers into micelles was investigated by light scattering, fluorescence spectroscopy, and cryo-TEM. These ELP_{BC}'s undergo two phase transitions as a function of solution temperature: a unimer-to-spherical micelle transition at an intermediate temperature and a micelle-to-bulk aggregate transition at a higher temperature when the hydrophilic-to-hydrophobic block ratio is between 1:2 and 2:1. The critical micelle temperature is controlled by the length of the hydrophobic block, and the size of the micelle is controlled by both the total ELP_{BC} length and hydrophilic-to-hydrophobic block ratio. These polypeptide micelles display a critical micelle concentration in the range 4−8 μM demonstrating the high stability of these structures. These studies have also identified a subset of ELP_{BC}'s bearing terminal peptide ligands that are capable of forming multivalent spherical micelles that present multiple copies of the ligand on their corona in the clinically relevant temperature range 37−42 °C and target cancer cells. These ELP_{BC}'s may be useful for drug targeting by thermally triggered multivalency. More broadly, the design rules uncovered by this study should be applicable to the design of other thermally reversible nanoparticles for diverse applications in medicine and biology.

Introduction

Molecular self-assembly describes the spontaneous association of molecules under equilibrium conditions into well-defined stable aggregates joined by noncovalent bonds.[1] One of the simplest examples of self-assembly by polymers is demonstrated by linear AB diblock copolymers with a large solubility difference between the two blocks.[2,3] When an amphiphilic AB diblock copolymer is placed in a solvent that is only good for one block, an attractive and a repulsive force is generated that results in microphase separation[4] and self-assembly of individual molecules into supramolecular structures. For amphiphilic AB diblock copolymers, self-assembly often results in the formation of a spherical micelle consisting of a core made up of an insoluble block that is shielded from the solvent by a hydrated corona composed of a more soluble block.[2] Other structures such as cylindrical micelles, toroids, lamellar sheets, or vesicles can also be formed, and the formation of these structures depends on the length of the A and B segments relative to each other.[5] Bioinspired amphiphilic molecules that exhibit this behavior range from simple di- or tripeptides[6,7] to more complex, naturally occurring peptide motifs such as coiled-coils (i.e., "leucine zipper"),[8−10] collagen, elastin-like polypeptides (ELPs),[11,12] silk-like polypeptides,[13] and combinations thereof,[14] as well as conjugates of peptides with alkyl chains (i.e., peptide amphiphiles).[15]

[†] Duke University.
[‡] National Institutes of Health.
[§] Johannes Gutenberg-Universität.

(1) Whitesides, G. M.; Mathias, J. P.; Seto, C. T. *Science* **1991**, *254*, 1312−1319.
(2) Rodriguez-Hernandez, J.; Checot, F.; Gnanou, Y.; Lecommandoux, S. *Prog. Polym. Sci.* **2005**, *30*, 691−724.
(3) Riess, G. *Prog. Polym. Sci.* **2003**, *28*, 1107−1170.
(4) Forster, S.; Plantenberg, T. *Angew. Chem., Int. Ed.* **2002**, *41*, 689−714.
(5) Thomas, E. L. *Science* **1999**, *286*, 1307−1307.
(6) Zhang, S. G. *Nat. Biotechnol.* **2003**, *21*, 1171−1178.
(7) Caplan, M. R.; Schwartzfarb, E. M.; Zhang, S. G.; Kamm, R. D.; Lauffenburger, D. A. *Biomaterials* **2002**, *23*, 219−227.
(8) Xu, C. Y.; Breedveld, V.; Kopecek, J. *Biomacromolecules* **2005**, *6*, 1739−1749.
(9) Petka, W. A.; Harden, J. L.; McGrath, K. P.; Wirtz, D.; Tirrell, D. A. *Science* **1998**, *281*, 389−392.
(10) Zimenkov, Y.; Dublin, S. N.; Ni, R.; Tu, R. S.; Breedveld, V.; Apkarian, R. P.; Conticello, V. P. *J. Am. Chem. Soc.* **2006**, *128*, 6770−6771.
(11) Meyer, D. E.; Chilkoti, A. *Biomacromolecules* **2002**, *3*, 357−367.
(12) Nagapudi, K.; Brinkman, W. T.; Leisen, J.; Thomas, B. S.; Wright, E. R.; Haller, C.; Wu, X. Y.; Apkarian, R. P.; Conticello, V. P.; Chaikof, E. L. *Macromolecules* **2005**, *38*, 345−354.
(13) Altman, G. H.; Diaz, F.; Jakuba, C.; Calabro, T.; Horan, R. L.; Chen, J. S.; Lu, H.; Richmond, J.; Kaplan, D. L. *Biomaterials* **2003**, *24*, 401−416.

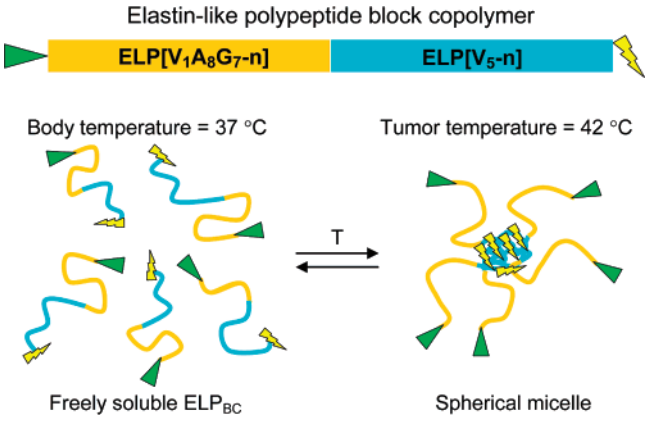

Figure 1. Temperature triggered self-assembly of an ELP_{BC} to form multivalent spherical micelles. An N-terminal ELP[$V_1A_8G_7$-*n*] gene (hydrophilic, high T_t) and C-terminal ELP[V_5-*n*] gene (hydrophobic, low T_t) are seamlessly fused together to create a gene that encodes an ELP_{BC}. When the size and ratio of the blocks are correctly selected, the ELP_{BC} self-assembles into a spherical micelle at ~40 °C. In the cartoon shown, upon self-assembly the spherical micelles present multiple copies of an affinity targeting moiety (green triangle) and sequester a drug or imaging agent (lightning bolt) within the core of the micelle.

In contrast to the spontaneous self-assembly of block copolymers into supramolecular structures, we are interested in the design of "smart"—stimuli-responsive—peptide-based block copolymers[11,12,14,16−19] that can be *triggered to self-assemble by a relatively small change in solution conditions*. We are especially interested in the challenge of designing polymers that can be triggered to self-assemble in response to clinically relevant intrinsic stimuli, such as the difference in pH between normal tissues (~7.4) and the tumor microenvironment (6.5−6.8)[20] and differences in calcium concentration between the extracellular and intracellular environment,[21,22] or extrinsic stimuli, such as the elevated temperature employed in mild hyperthermia treatment of solid tumors.[23] This interest is motivated by the recognition that nanoparticles that can self-assemble *in vivo* by physiologically or clinically relevant triggers have enormous applications in the emerging field of nanomedicine.[15,24−26]

In our first attempt at the design of triggered self-assembled nanoparticles, we have focused on the synthesis of a polypeptide that can be triggered to self-assemble into a spherical micelle by a small increase of temperature to between 37 and 42 °C, the temperature range approved for clinical application of hyperthermia.[23] We chose elastin-like polypeptides (ELPs) as the peptide building block of these AB diblock copolymers to explore the feasibility of this goal. ELPs are genetically encoded biopolymers of the pentameric repeat Val-Pro-Gly-Xaa-Gly where Xaa, termed the guest residue, is any amino acid besides proline.[27] The choice of ELPs as the building blocks for these systems was dictated by the following reasons. First, ELPs exhibit inverse temperature phase transition behavior (also called a lower critical solution temperature transition [LCST]); they are soluble at temperatures below their transition temperature (T_t) but become insoluble and aggregate at temperatures above their T_t.[27−29] Their T_t is tuned by adjusting the guest residue composition, molecular weight (MW), and ELP concentration.[11,30,31] This feature of ELPs is useful because it allows us to begin the design of temperature triggered self-assembling polymers using a repeat motif that is intrinsically responsive to its environment. Second, ELPs are not solely responsive to temperature; the phase transition of ELPs can also be triggered by ionic strength, pH, and light.[29,32] However, the use of these triggers in the context of self-assembly, as opposed to coacervation,[33] only has a few precedents.[11,34,35] We emphasize that, for such systems to move beyond proof-of-principle and be useful in the emerging field of nanomedicine, triggered self-assembly by physiologically relevant triggers is essential and is, thus, the driving force behind this study.

We synthesized a series of ELP block copolymers (ELP_{BC}'s) in a linear AB diblock architecture by seamlessly fusing an N-terminal ELP gene with a high T_t (T_t > 90 °C, more hydrophilic Xaa) to a C-terminal ELP gene with a much lower T_t ($T_t \approx$ 40 °C, more hydrophobic Xaa), as shown in Figure 1. These ELP_{BC}'s are highly soluble at a solution temperature below the T_t of both ELP blocks. However, upon an increase in solution temperature, we hypothesized that ELP_{BC}'s would self-assemble into a spherical micelle when the low T_t block undergoes its inverse temperature phase transition.[11] In this study, we synthesized 10 ELP_{BC}'s of various overall lengths (i.e., MWs) and hydrophilic-to-hydrophobic block MW ratios to (1) determine a fundamental set of design rules that results in the self-assembly of ELP_{BC}'s into defined structures; (2) isolate a construct that self-assembles into a multivalent spherical micelle within a clinically relevant hyperthermic temperature range of 37 to 42 °C; and (3) determine the physical properties of these self-assembled constructs.

Materials and Methods

Nomenclature. The different ELP constructs are named using the notation ELP[$X_iY_jZ_k$-*n*].[11] The bracketed capital letters are the single

(14) Megeed, Z.; Cappello, J.; Ghandehari, H. *Adv. Drug Delivery Rev.* **2002**, *54*, 1075−1091.
(15) Hartgerink, J. D.; Beniash, E.; Stupp, S. I. *Proc. Natl. Acad. Sci. U.S.A.* **2002**, *99*, 5133−5138.
(16) Cappello, J.; Crissman, J.; Dorman, M.; Mikolajczak, M.; Textor, G.; Marquet, M.; Ferrari, F. *Biotechnol. Prog.* **1990**, *6*, 198−202.
(17) McGrath, K. P.; Fournier, M. J.; Mason, T. L.; Tirrell, D. A. *J. Am. Chem. Soc.* **1992**, *114*, 727−733.
(18) Bellomo, E. G.; Wyrsta, M. D.; Pakstis, L.; Pochan, D. J.; Deming, T. J. *Nat. Mater.* **2004**, *3*, 244−248.
(19) Rodriguez-Cabello, J. C.; Reguera, J.; Girotti, A.; Arias, F. J.; Alonso, M. Genetic engineering of protein-based polymers: The example of elastinlike polymers. *Ordered Polymeric Nanostructures At Surfaces*; Springer-Verlag: Berlin, 2006; Vol. 200, pp 119−167.
(20) Cardone, R. A.; Casavola, V.; Reshkin, S. J. *Nat. Rev. Cancer* **2005**, *5*, 786−795.
(21) Brown, E. M. *Physiol. Rev.* **1991**, *71*, 371−411.
(22) Brown, E. M.; Quinn, S. M.; Vassilev, P. M. The Plasma Membrane Calcium Sensor. In *Calcium as a Cellular Regulator*; Carafoli, E., Klee, C., Eds.; Oxford University Press: New York, 1999.
(23) Dewhirst, M. W.; Jones, E.; Samulski, T.; Vujaskovic, Z.; Li, C. Y.; Prosnitz, L. Hyperthermia. In *Cancer Medicine 6*; Kufe, D., Pollack, R., Weichselbaum, R., Bast, R., Gansler, T., Holland, J., Frei, E., Eds.; B.C. Decker: Hamilton, Canada, 2003; pp 623−636.
(24) Silva, G. A.; Czeisler, C.; Niece, K. L.; Beniash, E.; Harrington, D. A.; Kessler, J. A.; Stupp, S. I. *Science* **2004**, *303*, 1352−1355.
(25) Lee, E. S.; Na, K.; Bae, Y. H. *J. Control. Release* **2005**, *103*, 405−418.
(26) Liu, S. Q.; Wiradharma, N.; Gao, S. J.; Tong, Y. W.; Yang, Y. Y. *Biomaterials* **2007**, *28*, 1423−1433.
(27) Urry, D. W. *Prog. Biophys. Mol. Biol.* **1992**, *57*, 23−57.
(28) Li, B.; Alonso, D. O. V.; Bennion, B. J.; Daggett, V. *J. Am. Chem. Soc.* **2001**, *123*, 11991−11998.
(29) Urry, D. W. *J. Phys. Chem. B* **1997**, *101*, 11007−11028.
(30) Meyer, D. E.; Chilkoti, A. *Biomacromolecules* **2004**, *5*, 846−851.
(31) Urry, D. W.; Luan, C. H.; Parker, T. M.; Gowda, D. C.; Prasad, K. U.; Reid, M. C.; Safavy, A. *J. Am. Chem. Soc.* **1991**, *113*, 4346−4348.
(32) Alonso, M.; Reboto, V.; Guiscardo, L.; San Martin, A.; Rodriguez-Cabello, J. C. *Macromolecules* **2000**, *33*, 9480−9482.
(33) Zhang, Y. J.; Trabbic-Carlson, K.; Albertorio, F.; Chilkoti, A.; Cremer, P. S. *Biomacromolecules* **2006**, *7*, 2192−2199.
(34) Lee, T. A. T.; Cooper, A.; Apkarian, R. P.; Conticello, V. P. *Adv. Mater.* **2000**, *12*, 1105−1110.
(35) Sallach, R. E.; Wei, M.; Biswas, N.; Conticello, V. P.; Lecommandoux, S.; Dluhy, R. A.; Chaikof, E. L. *J. Am. Chem. Soc.* **2006**, *128*, 12014−12019.

amino acid code specifying the guest residues in the ELP sequence, and the subscripts designate the number of Val-Pro-Gly-Xaa-Gly repeats for each corresponding guest residue in the monomer gene. *n* represents the number of pentapeptides. All ELP_{BC}'s herein are composed of an N-terminal ELP[$V_1A_8G_7$-*n*] gene followed by a C-terminal ELP[V_5-*n*] gene. The ELP[$V_1A_8G_7$-*n*] gene has a monomer repeat unit of 16 pentapeptides, and ELP[V_5-*n*] has a monomer repeat unit of 5 pentapeptides. For semantic clarity, all ELP_{BC} genes are named using the notation ELP-*x*/*y* where *x* is the number of pentapeptides for the ELP[$V_1A_8G_7$-*n*] gene and *y* is the number of pentapeptides for the ELP-[V_5-*n*] gene. For example, ELP-64/90 is composed of an N-terminal ELP[$V_1A_8G_7$-64] and C-terminal ELP[V_5-90]. Because ELP[$V_1A_8G_7$-*n*] and ELP[V_5-*n*] have different lengths of their basic repeat unit, approximate hydrophilic-to-hydrophobic block ratios are rounded to the nearest consistent number. For example, ELP-64/90 has a reported hydrophilic-to-hydrophobic block ratio of 2:3.

A complete materials and methods section may be found in the Supporting Information.

Results and Discussion

The goals of these studies were to (1) discover the design rules for the self-assembly of ELP_{BC}'s into nanomesoscale structures; (2) isolate a construct that self-assembles into a multivalent micelle within the clinically relevant hyperthermic temperature range 37 to 42 °C; and (3) determine the physical properties of these micelles. To accomplish these goals, we synthesized a series of 10 ELP_{BC}'s with various MWs and hydrophilic-to-hydrophobic ratios and examined their self-assembly with DLS, SLS, fluorescence spectroscopy, and cryo-TEM. Finally, an ELP_{BC} that formed stable micelles in the range 37−42 °C was then modified at the gene level to present an RGD or NGR peptide, and these ligand-functionalized ELP_{BC}'s were further characterized by light scattering to investigate their ability to self-assemble into multivalent nanoparticles in the desired range 37−42 °C.

Thermal Properties of ELP_{BC}'s. Single segment ELPs undergo a unimer-to-aggregate transition when heated above their T_t, producing a sharp (1−2 °C) increase in turbidity of an ELP solution.[11,30] In contrast, some ELP_{BC}'s exhibited a two-step thermal response; the ELP_{BC} solution was transparent at low temperatures (<36 °C), but as the temperature was increased, the absorbance increased and remained elevated above baseline levels (range = 36−46 °C) (Figure 2). Upon further heating, the solution turbidity increased sharply and plateaued (range = 49−51 °C) at a constant value. We believe that the first small increase in absorbance was caused by the inverse temperature phase transition of the low T_t ELP block (T_{t1}). Upon heating above 49 °C, the high T_t ELP block underwent its inverse temperature phase transition (T_{t2}) which induced the formation of large aggregates indicated by the high OD value. T_{t1} was defined as the temperature at which the OD first deviated from the baseline, and T_{t2} was defined as the temperature at the maximum in the derivative of OD with respect to temperature (dOD/d*T*).

We believe this two-step change in turbidity is caused by a monomer−micelle transition followed by a micelle−coacervate transition characterized by the formation of micron-sized aggregates. Previous experiments by our laboratory have demonstrated that a small increase in absorbance, as shown in Figure 2 from 36−46 °C, is indicative of the formation of nanoparticles (defined as a diameter < 100 nm).[11] This finding motivated the screening of all 10 ELP_{BC}'s with fixed-angle DLS,

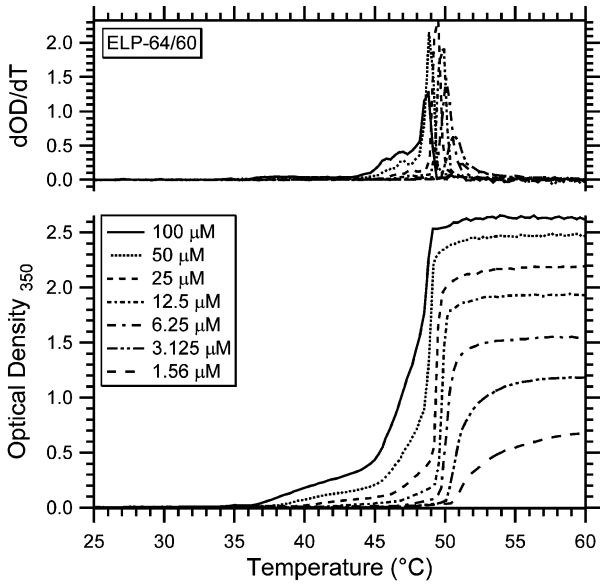

Figure 2. Turbidity profile of ELP-64/60 at various concentrations as a function of temperature. Turbidity profiles were obtained by monitoring optical density (OD) at 350 nm in PBS as the solution was heated at a rate of 1 °C/min. The increase in OD indicates formation of ELP particles larger than an ELP unimer. The sharpness of the micelle-to-aggregate transition can be obtained from dOD/d*T* as shown in the top portion of this figure.

which indicated that 6 out of 10 ELP_{BC}'s formed nanoparticles. These screening experiments also revealed that ELP_{BC}'s with a hydrophilic-to-hydrophobic ratio between 1:2 and 2:1 formed nanoparticles (1:2 ≤ ratio ≤ 2:1). This lower threshold of a 1:2 ratio is similar to an *f* value of 33%, which was shown by Discher et al.[36] to form vesicles. Increasing the hydrophilic-to-hydrophobic ratio above 1:2 also resulted in nanoparticle formation, analogous to Discher's findings.[36] However, ratios exceeding 2:1 did not form nanoparticles and instead behaved as a simple monoblock ELP, only exhibiting a single transition from unimer to micron-sized aggregates. This result is likely due to an insufficient solubility difference between the blocks to self-assemble into a nanoparticle.

The concentration dependence of T_{t1} and T_{t2} was determined for the six ELP_{BC}'s that formed nanoparticles (Figure 3). Both T_t's were fit as a logarithmic function of concentration, shown as a solid line in Figure 3. Similar to simple monoblock ELPs, T_{t1} had a decreasing logarithmic dependence on ELP concentration.[30] Furthermore, T_{t1} appeared to scale with the T_t of the parent ELP[V_5-*n*] block (see the dashed lines in Figure 3). For example, the average T_{t1} for each ELP_{BC} with an ELP[V_5-60] block was consistently 4.2 °C higher than that of the parent ELP[V_5-60], most likely due to the influence of the more hydrophilic ELP[$V_1A_8G_7$-*n*] on ELP[V_5-60]'s phase transition. This increase in T_t diminished to 1.5 and 1.2 °C for ELP_{BC}'s composed of ELP[V_5-90] and ELP[V_5-120], respectively. Therefore, these results suggested that T_{t1} is controlled by the length (i.e., MW) of the low T_t block (ELP[V_5-*n*]). In contrast, T_{t2} appeared independent of both ELP[$V_1A_8G_7$-*n*] and ELP[V_5-*n*] block lengths and had a much weaker dependence on concentration ($m = -0.55$ to -1.48 for T_{t2}, and $m = -1.59$ to -2.60 for T_{t1}). This relative lack of length dependence and weaker concentration dependence for the T_{t2} may be due to the close proximity of ELP[$V_1A_8G_7$-*n*] in the corona of the micelle,

(36) Discher, D. E.; Eisenberg, A. *Science* **2002**, *297*, 967−973.

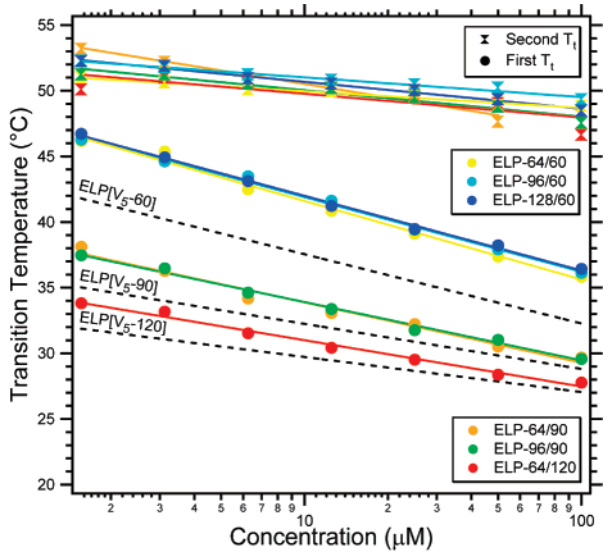

Figure 3. Dependence of transition temperature (T_t) on ELP_{BC} concentration for the six ELP_{BC}'s that formed nanoparticles in PBS. The first T_t is defined by the temperature at the first apparent increase in turbidity (filled circle). The second T_t is defined by the temperature at the maximum in dOD/dT (filled hourglass). Both the first and second T_t had a decreasing logarithmic dependence on ELP concentration. The dependence of T_t on ELP concentration was quantified by fitting these data with the following equation, $T_t = m \ln([ELP]) + b$, shown by a solid line. The parent ELP[V_5-n]'s thermal response is shown by the dashed line.

effectively maximizing its local concentration. The high local ELP concentration in the corona causes its T_{t2} to be independent of concentration, a trend also observed for monoblock ELPs at high concentrations.[29,30]

Light Scattering of ELP_{BC}'s. The temperature-dependent self-assembly of ELP_{BC}'s was next investigated by DLS performed at multiple angles to determine their size, CMT, polydispersity, and micelle formation temperature range. The ELP_{BC} unimers (R_h range = 5.3−9.8 nm) formed a monodisperse nanoparticle (R_h range = 29.1−39.9 nm) at a temperature near T_{t1}, as shown in Figure 4. This aggregation temperature determined by DLS was defined as the CMT. In some instances, the monodisperse nanoparticle was stable for 5 to 8 °C until a larger polydisperse aggregate (>1 μm) was formed, representing bulk aggregation after the corona block underwent its phase transition (Figure 4A). However, in other cases the monodisperse nanoparticle transitioned into a more polydisperse nanoparticle that grew in size until bulk aggregation was observed (Figure 4B). This transition from a monodisperse to polydisperse nanoparticle may be due to simple growth of a spherical aggregate or due to a sphere-to-rod transition. The stable monodisperse nanoparticles were classified as *type I nanoparticles* (Figure 4A), and the less stable nanoparticles were classified as *type II nanoparticles* (Figure 4B). This independent stratification of ELP_{BC}'s based on their phase transition behavior was structurally illuminating because all stable type I nanoparticles were composed of ELP[V_5-60] blocks and all type II nanoparticles were composed of ELP[V_5-n] blocks with lengths greater than 60 pentapeptides. The thermal properties of the ELP_{BC}'s, including their CMT and classifications are summarized in Table 1. Consistent with previous UV−visible spectrophotometry data, the CMT occurred about 4−6 °C higher than the parent ELP[V_5]'s T_t and this CMT was controlled by the length of the ELP[V_5] block.

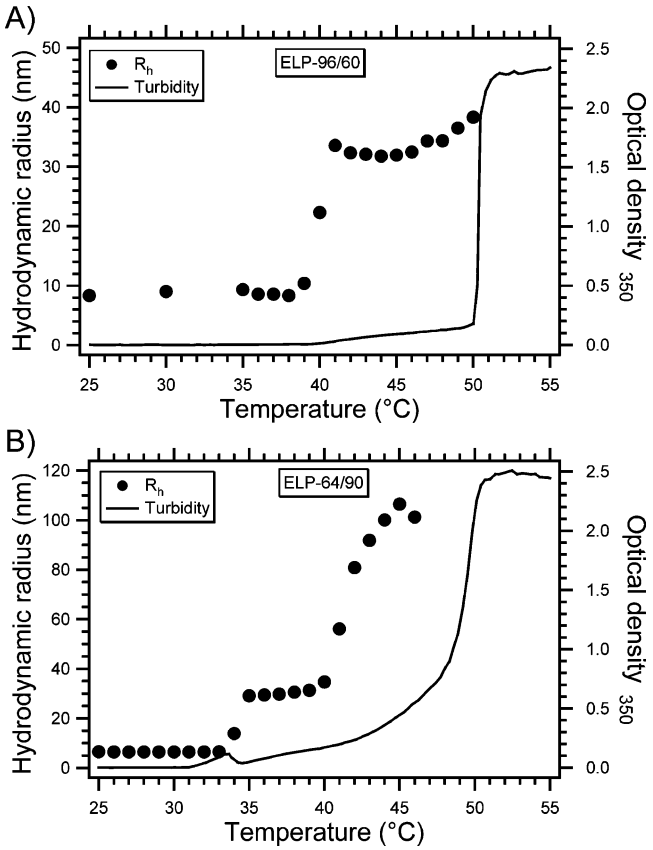

Figure 4. Hydrodynamic radius (R_h) and turbidity of (A) ELP-96/60 and (B) ELP-64/90 versus temperature. The DLS data were acquired at a 50° angle in PBS at a 25 μM ELP concentration. The R_h is displayed as the fast mode of a biexponential fit at temperatures below the first T_t and from a monoexponential fit at temperatures above the first T_t.

Table 1. Summary of ELP_{BC} Physical and Thermal Properties[a]

ELP	MW (kDa)	length (pentapeptides)	~ratio	CMT (°C)	ELP[V_5-n] T_t(°C)	type
ELP-64/60	49.4	124	1:1	42	36	type I
ELP-96/60	63.1	156	3:2	41	36	type I
ELP-128/60	75.1	188	2:1	42	36	type I
ELP-64/90	62.8	154	2:3	35	31	type II
ELP-96/90	73.9	186	1:1	36	31	type II
ELP-64/120	74.1	184	1:2	33	29	type II

[a] The data are listed in order of increasing low T_t block length. ELP[V_5-n]'s T_t is defined as the maximum in dOD/dT for the parent ELP[V_5-n] block from an upward thermal ramp (1 °C/min) in PBS at 25 μM. The type refers to the stability of the nanoparticle (see text for discussion).

To further elucidate the structure and polydispersity of these ELP_{BC} nanoparticles, DLS and SLS at multiple angles were performed at a temperature within the stable nanoparticle temperature range. The R_g, MW_{app}, and Z of each ELP_{BC} were determined with SLS. The structure of the ELP_{BC} nanoparticle was characterized further by combining the DLS and SLS data together to calculate the ρ ratio ($\rho = R_g/R_h$). The ρ ratio equals 0.775 for a homogeneous hard sphere (e.g., spherical micelle), 1.0 for a thin hard spherical shell (e.g., vesicle), 1.504 for a random monodisperse coil in a θ solvent, and 1.73 for a random monodisperse coil in a good solvent (it is important to note that polydispersity will increase the ρ ratio because large molecules of a broad distribution will contribute more to R_g than R_h provided that internal modes of motion are absent).[37,38]

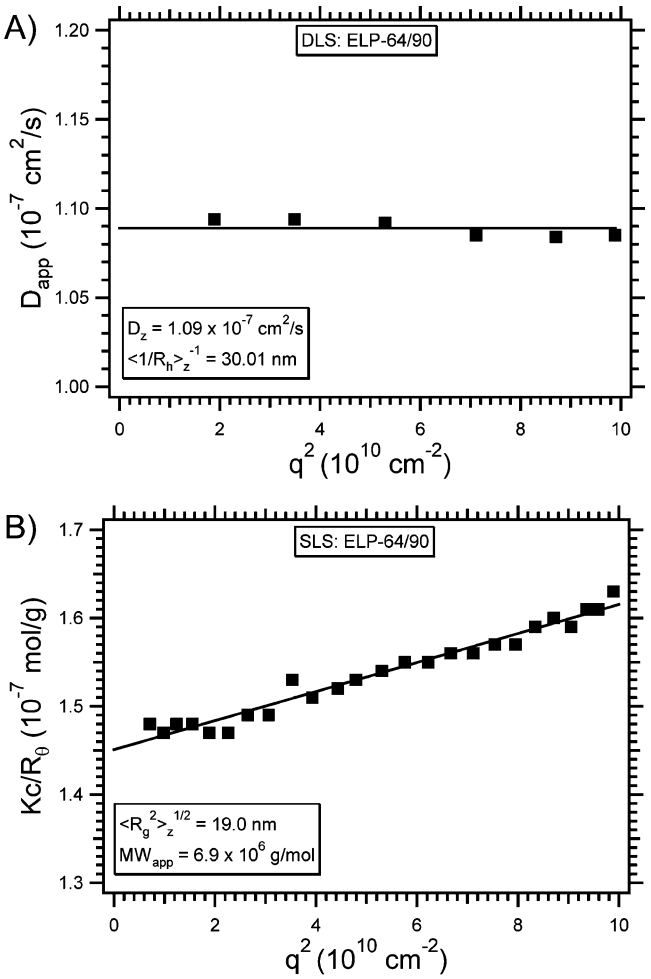

Figure 5. (A) dynamic light scattering (DLS) and (B) static light scattering (SLS) collected at multiple angles for ELP64/90 in PBS at 37 °C and an ELP_{BC} concentration of 25 μM. Angle is expressed as the absolute value of the scattering vector (q) squared. (A) DLS reveals no angular dependence of apparent diffusion coefficient (D_{app}) indicated by the solid line plotted with a slope of zero. The graph is displayed with ±10% of the mean D_{app} value. The z-averaged diffusion coefficient (D_z) is the average of all six measurements, and the hydrodynamic radius (R_h) is calculated from the Stokes−Einstein equation. (B) The radius of gyration (R_g) and apparent molecular weight (MW_{app}) were determined with SLS by calculating the slope and intercept of the solid line relating the inverse of the scattered intensity to q^2.

An example of DLS and SLS analysis is shown in Figure 5 for ELP-64/90. In general, nanoparticles in this size range are considered to be a monodisperse sphere if their D_{app} does not vary by more than 10% (positive sloped line) of the mean D_{app} as the form factor ($P(q)$) is highly dependent upon the scattering angle.[39] This ELP_{BC} nanoparticle (R_h = 30 nm) was a monodisperse hard sphere as indicated by the lack of angular dependency of D_{app} in the DLS data (Figure 5A).[39−41] The R_g (19.0 nm), MW_{app} (6.9 × 10^6), and Z (110) of this ELP_{BC} nanoparticle were determined with SLS as shown in Figure 5B. The ρ ratio for ELP-64/90 was 0.633, indicating that the nanoparticle was a hard sphere and therefore a spherical micelle. A summary of the properties of each nanoparticle-forming ELP_{BC} including R_h, R_g, MW_{app}, ρ ratio, and Z is shown in Table 2.

Table 2. Summary of ELP_{BC} Micelle Properties[a]

ELP	length	~ratio	R_h (nm)	R_g (nm)	ρ	MW_{app} (10^6)	Z	CMC (μM)
ELP-64/60	124	1:1	29.1	20.7	0.712	2.8	57	6.3 ± 0.55
ELP-64/90	154	2:3	30.0	19.0	0.633	6.9	110	8.1 ± 0.64
ELP-96/60	156	3:2	32.0	22.0	0.687	5.9	94	6.2 ± 0.95
ELP-64/120	184	1:2	39.9	30.0	0.753	8.6	116	7.9 ± 1.2
ELP-96/90	186	1:1	36.6	26.5	0.724	9.8	133	5.6 ± 0.97
ELP-128/60	188	2:1	34.3	24.0	0.701	4.2	56	4.4 ± 0.64

[a] The data are listed in order of increasing length expressed in number of pentapeptides. CMC is displayed as mean ± SD (n = 3).

These data in Table 2 prove that ELP_{BC}'s with a hydrophilic-to-hydrophobic ratio between 1:2 and 2:1 form a monodisperse spherical micelle at a temperature between T_{t1} and T_{t2}. In addition, the size of the micelle was controlled by both the total length of the ELP_{BC} and the hydrophilic-to-hydrophobic block ratio supported by the models of Israelachvili et al.[42] and Discher et al.[36] For example, increasing the total length while maintaining a constant block ratio increased the micelle size from 29.1 nm for ELP-64/60 (length = 120) to 36.6 nm for ELP-96/90 (length = 180). Furthermore, increasing the hydrophobic block length relative to the hydrophilic block increased the micelle size for an ELP_{BC} with a constant length due to the increased hydrophobic volume fraction. Although the ρ ratios (range = 0.633 to 0.753) were slightly lower than the theoretical value of 0.775, they further confirm the formation of a hard spherical micelle structure. These lower values may be due to inhomogeneous packing within the micelle in the radial direction. The high aggregation numbers (Z = 56−133) suggest that a sufficient number of targeting ligands may be presented in the micelle's corona to enhance the binding avidity.

Fluorescence Characterization of ELP_{BC}'s. The CMC was determined using fluorescence spectroscopy and pyrene, a fluorescent probe sensitive to the polarity of its microenvironment. The ratio of the first and third peaks (I_1/I_3) of the monomer emission spectrum decreases as the probe partitions into a less polar region such as a micelle's hydrophobic core. For an ELP-64/90 solution, this ratio remained relatively constant at temperatures below its CMT (T = 20−35 °C) as shown in Figure 6A. At temperatures between T_{t1} and T_{t2}, the ratio monotonically decreased until it reached a minimum at T_{t2} (T = 50 °C) indicating that the overall polarity of the micelle decreased throughout the micelle temperature range. There was a slight increase in the average polarity of the solution at temperatures above the bulk aggregation temperature (T > 50 °C) suggesting that pyrene partitioned into a more aqueous environment. Similar findings by Chung et al. were interpreted as release of the entrapped molecule from thermoresponsive micelles.[43] The CMC was determined by plotting the minimum of the I_1/I_3 ratio from 35 to 45 °C (see Figure 6A) as a function of ELP_{BC} concentration (Figure 6B). The inflection point of a sigmoid fit to data in this temperature range was defined as the CMC. The CMC was determined for all six ELP_{BC}'s capable of forming

(37) Burchard, W. Solution properties of branched Macromolecules. In *Branched Polymers Ii*; Springer-Verlag: Berlin, 1999; Vol. 143, pp 113−194.
(38) Burchard, W.; Schmidt, M.; Stockmayer, W. H. *Macromolecules* **1980**, *13*, 1265−1272.
(39) Schmidt, M.; Burchard, W.; Ford, N. C. *Macromolecules* **1978**, *11*, 452−454.
(40) Antonietti, M.; Heinz, S.; Schmidt, M.; Rosenauer, C. *Macromolecules* **1994**, *27*, 3276−3281.
(41) Schmidt, M.; Stockmayer, W. H. *Macromolecules* **1984**, *17*, 509−514.
(42) Israelachvili, J. *Intermolecular & surface forces*, 2nd ed.; Academic Press: New York, 1991.
(43) Chung, J. E.; Yokoyama, M.; Yamato, M.; Aoyagi, T.; Sakurai, Y.; Okano, T. *J. Control. Release* **1999**, *62*, 115−127.

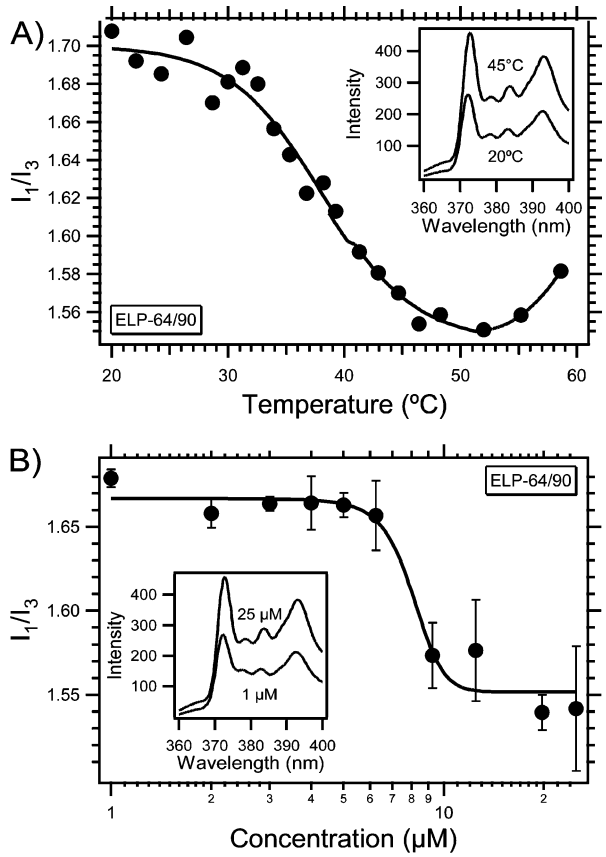

Figure 6. Dependence of pyrene fluorescence on (A) temperature and (B) concentration for 25 μM ELP-64/90 in PBS. (A) I_1/I_3 of pyrene decreased from 20 to 60 °C indicating a reduction in the polarity of the ELP-64/90 solution. There was a pronounced decrease in I_1/I_3 at temperatures above the CMT and below the second transition. (B) I_1/I_3 at the inflection point of each temperature scan (as shown in (A) was plotted as a function of ELP-64/90 concentration. The inflection point of a sigmoid fit (solid line) was defined as the CMC. Data are the mean ± SD in (B) ($n = 3$).

nanoparticles (Table 2). The I_1/I_3 ratio remained constant at low concentrations of ELP-64/90 but decreased to a lower value as the concentration was increased. These data demonstrate that ELP-64/90 micelles formed at a low concentration of 8.1 μM. Furthermore, all six of the nanoparticle-forming ELP_{BC}'s have a CMC < 10 μM, implying that ELP_{BC} micelles are quite stable structures.[44]

The microviscosity of the micelles was further investigated with fluorescence spectroscopy using a fluorescent PC_3P probe.[45,46] The emission spectrum of this probe has two characteristic peaks representing the contribution from monomer and excimer forms of the probe. The ratio of these two peaks (I_E/I_M) is proportional to the microviscosity of PC_3P's environment; PC_3P molecules with restricted motion will form intramolecular excimers while freely rotating PC_3P molecules will remain in monomer form. At solution temperatures below the first T_t, the microviscosity of an ELP-64/90 solution is similar to that of a control ELP[$V_5A_2G_3$-150], as shown in Figure 7 ($T = 30-40$ °C). The microviscosity increased within the micelle temperature range ($T = 40-50$ °C) as indicated by the higher I_E/I_M of an ELP-64/90 solution. The control ELP[$V_5A_2G_3$-150]

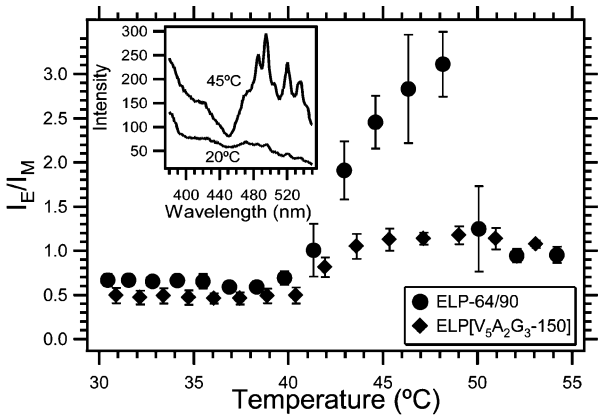

Figure 7. PC_3P I_E/I_M ratio as a function of temperature for ELP-64/90 in PBS at 25 μM. This ratio increased at the CMT of ELP-64/90 (~40 °C) and at the bulk aggregation temperature for the control ELP[$V_5A_2G_3$-150] (~42 °C), indicating a greater microviscosity in the microenvironment of PC_3P. The I_E/I_M ratio decreased at the second T_t of ELP-64/90 (~50 °C). Data are mean ± SD ($n = 3$).

exhibited a lower microviscosity than the micelle after it underwent its inverse temperature phase transition ($T_t = 42$ °C) into a bulk aggregate. Furthermore, the ELP-64/90 solution demonstrated a similar microviscosity to the control ELP-[$V_5A_2G_3$-150] after it underwent bulk aggregation at 50 °C. These data suggest that the core of an ELP_{BC} micelle had a greater microviscosity than both a soluble ELP solution and an ELP bulk aggregate. Also, a reduction of microviscosity as the ELP_{BC} goes through its micelle-to-aggregate transition suggests that the micelles reorganize their structure during their transition to a bulk aggregate.

Cryo-TEM of ELP_{BC}'s. The micellar structures of these ELP_{BC}'s were further validated by cryo-TEM obtained using a vitrified ELP_{BC} sample in the nanoparticle phase. A selected set of ELP_{BC} micelle images are shown in Figure 8. The homogeneous intensity throughout the interior of the nanoparticles is indicative of a micellar structure.

Self-Assembly of Ligand-Functionalized ELP_{BC}'s. ELP_{BC}'s that formed stable, *type I* spherical micelles between 37 and 42 °C (ELP-64/60 and ELP96/60) were selected as candidates to create temperature triggered multivalent nanoparticles. We chose two different peptide motifs, the RGD and NGR tripeptides, as ligands to be presented in the corona following micelle self-assembly. These peptide sequences were selected because they are known targeting ligands for angiogenic tumor vasculature[47,48] and multivalent presentation of these ligands can improve tumor targeting and therapy.[49,50]

The self-assembly of ligand-targeted ELP_{BC}'s was compared to that of their parent ELP_{BC}'s (i.e., same ELP_{BC} without an N-terminal ligand) using DLS as shown in Figure 9. Importantly, DLS verified that ELP_{BC}'s with targeting ligands incorporated into their N-terminus also formed micelles of a similar size and

(44) Torchilin, V. P. *J. Control. Release* **2001**, *73*, 137−172.
(45) Chung, J. E.; Yokoyama, M.; Okano, T. *J. Control. Release* **2000**, *65*, 93−103.
(46) Kwon, G. S.; Naito, M.; Yokoyama, M.; Okano, T.; Sakurai, Y.; Kataoka, K. *Langmuir* **1993**, *9*, 945−949.
(47) Brooks, P. C.; Clark, R. A. F.; Cheresh, D. A. *Science* **1994**, *264*, 569−571.
(48) Pasqualini, R.; Koivunen, E.; Kain, R.; Lahdenranta, J.; Sakamoto, M.; Stryhn, A.; Ashmun, R. A.; Shapiro, L. H.; Arap, W.; Ruoslahti, E. *Cancer Res.* **2000**, *60*, 722−727.
(49) Dijkgraaf, I.; Kruijtzer, J. A. W.; Liu, S.; Soede, A. C.; Oyen, W. J. G.; Corstens, F. H. M.; Liskamp, R. M. J.; Boerman, O. C. *Eur. J. Nucl. Med. Mol. Imaging* **2007**, *34*, 267−273.
(50) Pastorino, F.; Brignole, C.; Di Paolo, D.; Nico, B.; Pezzolo, A.; Marimpietri, D.; Pagnan, G.; Piccardi, F.; Cilli, N.; Longhi, R.; Ribatti, D.; Corti, A.; Allen, T. M.; Ponzoni, M. *Cancer Res.* **2006**, *66*, 10073−10082.

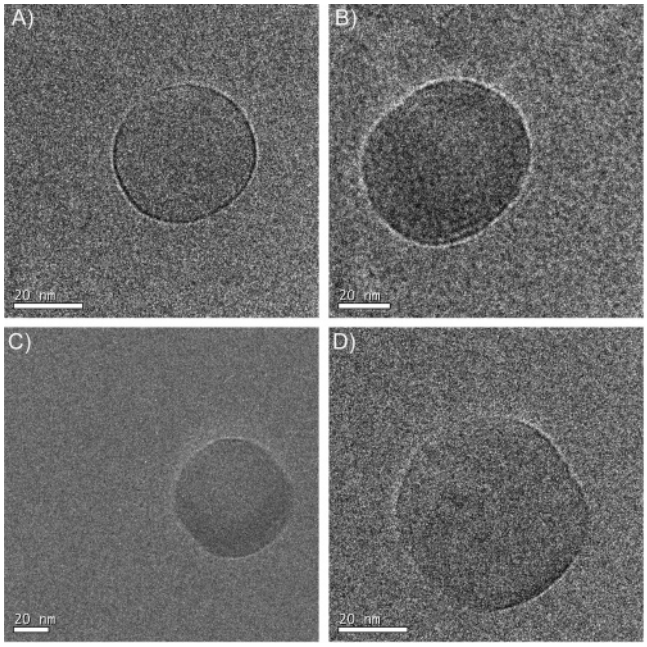

Figure 8. Cryo-TEM of (A) ELP-64/60, (B) ELP-96/90, (C) ELP-64/90, and (D) ELP-96/60 vitrified at a temperature that induced micelle formation in PBS at 25 μM. The bar is 20 nm in all images.

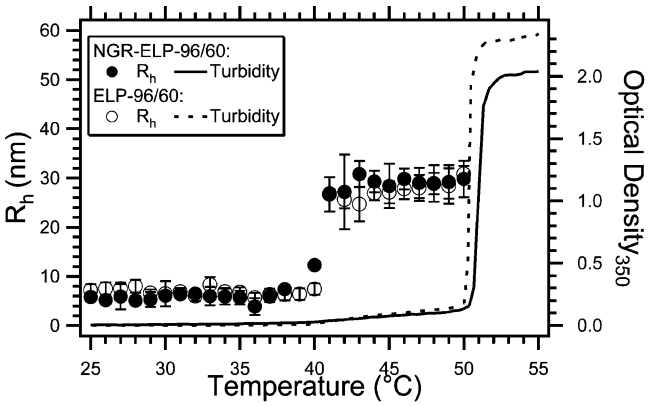

Figure 9. Hydrodynamic radius (R_h) and turbidity of ELP-96/60 (open symbols and dashed line) and NGR-ELP-96/60 (closed symbols and solid line) versus temperature in PBS at a 25 μM ELP concentration. The turbidity profile is shown from an upward thermal ramp (1 °C/min). DLS data were acquired at a fixed angle of 90° and a 25 μM ELP_{BC} concentration using a DynaPro LSR instrument. The autocorrelation function was analyzed using a cumulant and regularization algorithm for Rayleigh spheres provided by the manufacturer to determine the hydrodynamic radii. Data are reported as mean ± polydispersity.

in a similar temperature range as in the case of ELP_{BC}'s without targeting ligands, which suggest their utility for *in vivo* targeting. Furthermore, the fact that neither peptide ligand perturbed the temperature triggered self-assembly behavior of the ELP_{BC} suggests that this diblock copolymer system is highly tolerant to the incorporation of other peptide motifs for multivalent presentation. These results are notable because they suggest the feasibility of modular design of multivalent nanoparticles simply by swapping different peptide motifs, as well as the intriguing possibility of synthesizing multifunctional, multivalent nanoparticles by mixing several peptide-functionalized ELP_{BC}'s prior to thermally triggered self-assembly.

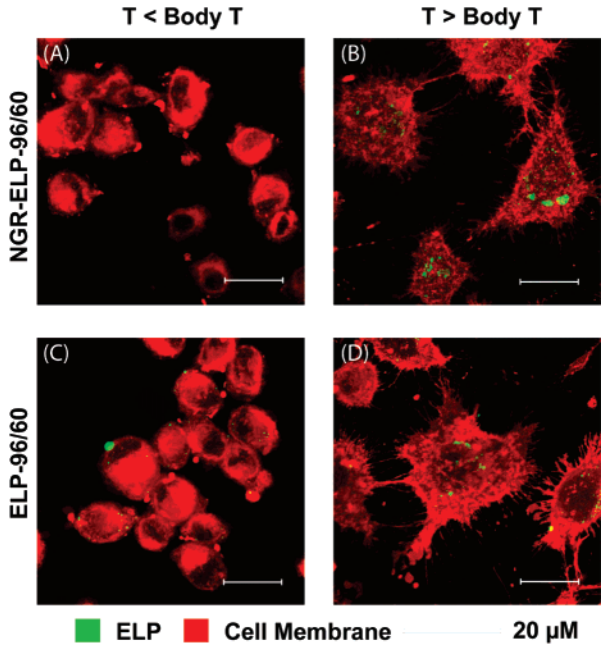

Figure 10. Confocal images illustrating the effects of heat and ligand presentation on cellular uptake of NGR-ELP-96/60-Alexa488 and ELP-96/60-Alexa488. Size bars represent 20 μM. NGR-ELP-96/60-Alexa488 (green) demonstrated limited accumulation in HT-1080 cells (red) in monovalent form (T < Body T, A) but accumulated in polyvalent micellar form (T > Body T, B). ELP-96/60 accumulated in the cell at low amounts in both monovalent (T < Body T, C) and polyvalent (T > Body T, D).

Cellular Uptake. Cellular uptake of NGR functionalized ELP_{BC}'s above and below body temperature was investigated with laser scanning confocal microscopy, shown in Figure 10. HT-1080 cells were used to examine internalization of NGR-functionalized ELP_{BC}'s because this cell line was positive for NGR's receptor, aminopeptidase N (APN)[51] (data not shown). Cells treated with ELP-96/60-Alexa488 and NGR-ELP-96/60-Alexa488 exhibited modest internalization and punctuate fluorescence at temperatures below body temperature (see Figure 10A and C), as has been shown previously.[52] Above body temperature, ELP-96/60-Alexa488 revealed a similar pattern of uptake as that for low temperature controls, but ligand-targeted NGR-ELP-96/60-Alexa488 demonstrated enhanced cellular uptake (see Figure 10B). The number of overlapping red-green pixels in the projection of NGR-ELP-96/60-Alexa488 was approximately 19-fold greater than that for unimers of NGR-ELP-96/60-Alexa488 (monovalent control) and 3.5-fold greater than that the micellar ELP-96/60-Alexa488 that did not present a NGR ligand (micelle control). These images suggest that micellar NGR-ELP-96/60-Alexa488 accumulated in cells to a greater extent than either unimeric NGR-ELP-96/60-Alexa488 or micellar ELP-96/60-Alexa488 controls.

Thermally Triggered Multivalent Targeting. The results presented here demonstrate that AB diblock polypeptides can be triggered to self-assemble into a spherical micelle in a narrow, clinically relevant temperature range of 37−42 °C. We envision the use of these polymers as multivalent carriers of drugs that self-assemble only in a defined region *in vivo*, such as a tumor

(51) Moffatt, S.; Wiehle, S.; Cristiano, R. J. *Hum. Gene Ther.* **2005**, *16*, 57−67.
(52) Dreher, M. R.; Raucher, D.; Balu, N.; Colvin, O. M.; Ludeman, S. M.; Chilkoti, A. *J. Control. Release* **2003**, *91*, 31−43.

heated with externally applied hyperthermia, to increase the drug carrier's binding affinity by converting it from a monovalent targeting agent to a multivalent nanoparticle. The increased affinity of the multivalent micelles relative to the unimer will selectively target the micelles to a specific tissue *in vivo* through high affinity interactions while minimizing background uptake of the unimer by normal tissues. We call this novel technique of controlling valency through triggered self-assembly *affinity modulated targeting*.

Affinity modulated targeting has three potential advantages over commonly used affinity targeted strategies,[53] especially within the context of cancer therapy: (1) the higher avidity of the nanoparticle to a heated tumor should localize more anticancer agents to that tumor; (2) the lower affinity in systemic circulation will reduce affinity to normal tissue, reducing systemic exposure; and (3) modulated affinity allows the targeting of more widely expressed tumor associated antigens. Tumor accumulation of an affinity targeted drug carrier appears to require a minimum threshold affinity of 10^{-7} M (K_D) and a maximum affinity ($\sim 10^{-9}$ M) above which tumor accumulation is not improved.[54] Affinity modulated targeting hence requires a low affinity ligand for a tumor receptor ($K_D \geq 10^{-7}$ M) when it is in its monovalent form. However, when an ELP_{BC} functionalized with this ligand self-assembles into a micelle that presents multiple copies of a ligand in a hyperthermic tumor, the avidity of the multivalent nanoparticle should theoretically increase between 10^3- and 10^8-fold from its monovalent affinity[55] and consequently result in maximal tumor accumulation ($K_D \leq 10^{-9}$ M). The low affinity in systemic circulation should reduce normal tissue exposure if the receptor is expressed in tissues other than the tumor. In addition, the selectively higher avidity within the tumor facilitates the use of tumor associated antigens that are ubiquitously expressed on many clinically relevant cancers, thus making this strategy potentially more widely applicable than other affinity targeting techniques incorporating a single tumor specific antigen.

(53) Allen, T. M. *Nat. Rev. Cancer* **2002**, *2*, 750−763.
(54) Adams, G. P.; Schier, R.; McCall, A. M.; Simmons, H. H.; Horak, E. M.; Alpaugh, R. K.; Marks, J. D.; Weiner, L. M. *Cancer Res.* **2001**, *61*, 4750−4755.
(55) Mammen, M.; Choi, S. K.; Whitesides, G. M. *Angew. Chem., Int. Ed.* **1998**, *37*, 2755−2794.

Conclusion

A series of 10 ELP_{BC}'s with a range of MWs and hydrophilic-to-hydrophobic ratios were recombinantly synthesized by recursive directional ligation of a monomer gene and plasmid-borne expression of the oligomerized gene in *E. coli*. ELP_{BC}'s with a hydrophilic-to-hydrophobic ratio between 1:2 and 2:1 formed monodisperse spherical micelles. The CMT was controlled by the length of the low T_t block and scaled with the parent ELP block's T_t. The size of the micelle was controlled by both the total ELP_{BC} length and hydrophilic-to-hydrophobic block ratio. These polypeptide micelles displayed a CMC in the range 4−8 μM, indicating that these structures are highly stable. Furthermore, the microviscosity of the ELP_{BC}'s increased as they self-assembled into a micelle from unimers. The microviscosity of the micelles was greater than the bulk aggregate, suggesting that the micellar structure was altered during reorganization into the micron size aggregates of the coacervate that occurred at the second thermal transition. The major findings of this study are that (1) it provides the first set of design rules for the self-assembly of AB diblock ELP copolymers into spherical micelles; (2) it has identified a set of ELP_{BC}'s that exhibit thermally triggered self-assembly into spherical micelles in the desired range 37−42 °C; and (3) it is the first demonstration of temperature triggered multivalency—that ELP_{BC}'s presenting biologically relevant peptide ligands at their termini self-assembled into spherical micelles at a clinically relevant temperature and target tumor cells. More broadly, the design rules uncovered by this study should be applicable to the design of other thermally reversible nanoparticles for diverse applications in medicine and biology.

Acknowledgment. This work was supported by Grants NIH EB-000188 (A.C.) and Sonderforschungsbereich 625 (M.S.). Matthew Dreher would like to acknowledge the Intramural Research Program of the National Institutes of Health for support. We thank Daniel Meyer for synthesis of some of the ELP genes and Michael Stepputat for assistance with the cryo-TEM.

Supporting Information Available: Experimental procedures can be found in the Supporting Information. This material is available free of charge via the Internet at http://pubs.acs.org.

JA0764862